Risk-based Optimal Distribution of Power Reserves in Wind Power Plants

Guzmán Díaz, Estefanía Planas, Jon Andreu, Javier Gómez-Aleixandre

Dep. of Electrical Engineering, University of Oviedo, Campus de Viesques, s/n, 33204 Spain

Dep. of Electrical Engineering, University of the Basque Country UPV/EHU, Alameda Urkijo, s/n, 48013 Spain

ABSTRACT

This paper employs the Conditional Value-at Risk, largely used in financial risk management, to specify the power reserve capacity of a wind power plant (WPP) under a risk metric. Evidences are shown here that other popular, simpler measure, the Value-at Risk, is inappropriate for that specification. Under this risk-based reserve metric, two programs are approached to optimally distribute a reserve request in a WPP subject to a given confidence level in the commitment. The most exhaustive of the two is a two-level formulation including a solution to the load power flow (LPF) in the WPP. By solving these two programs, for comparison with interior-point and heuristic solvers, conclusions are drawn. Notably, that a Pareto optimality occurs for stringent reserve requests; that putting off-line generators is financially more profitable than partial curtailments to respond to low reserve requests; and that in these cases accounting for losses through LPF-based optimization seems unnecessary.

KEYWORDS

Wind power; primary reserve; optimization; risk.

Correspondence

Dep. of Electrical Engineering, University of Oviedo,

Campus de Viesques, s/n, 33204 Spain

1. INTRODUCTION

The regulation of the frequency as an ancillary service is achieved through the response of economic markets and through the deployment of reliability reserves. This regulation takes place in different time scales following the occurrence of frequency changes derived from non-event or event processes. The non-event are related to the stochastic evolution of the demand and generation balance, being part of the optimal dispatch [1]. Contrarily, an event-derived response occurs as an unplanned contingency that moves the frequency away from its set-point.

In both processes, a common feature is precisely the emergence of an unbalance between generation and load. In the past, this issue was related almost exclusively to the oscillations of the demand and markets and, more severely, to the occurrence of $N-1$ events. However, the increasing penetration of wind energy has being notably degrading the system frequency, because in the end wind generation acts as a negative load with uncertain variability (see for instance the calculations in [2]). Consequently, more reserves have been put into consideration to cope with this variability [3].

The responsibility of controlling this frequency events was in the past assigned to all those generators with ramping or spinning capabilities; depending on the targeted reserve. But now, by way of compensation and in searching for a better balance, system operators (ISO) are asking for mandatory provisions of power reserves from wind power plants (WPP) as well [4], mainly targeting on FCR (frequency containment reserves) and possibly on FRR (frequency restoration reserves) [5]. See [6] for a discussion about regulatory issues, or [7] for particularization of the need for reserves in insular systems.

The provision of these reserves entails a cost to the WPP operator, however, because the generator must be unloaded following a curtailment curve that modifies the nominal wind speed to power conversion. This is a change in the conventional operation mode, in which the WPP produced at its maximum available power, following the maximum power point tracking. By contrast, what is suggested is that WPP can be regulated to achieve other strategic goals, such as the one presented on this paper; or, in general, favor the stable integration of sizable amount of wind energy in the system by strategically reducing the output of the WPP (see for instance [8]). The curtailment can be performed in a variety of ways: derated, relative spinning or percentage reserve, and absolute spinning or delta methods, are some [9, 10, 11, 12]. But in the end this assumes that the WPP will face a profit loss from curtailing its power production after obeying the the ISO requests.

Research efforts have been done towards analyzing WPP contribution to frequency support (see [3] for a review), also proposing different optimal algorithms that improve several aspects of the wind power conversion performance [13]. However, few works commit the sharing of power reserve among the turbines inside a WPP. In this sense, a reserve sharing that reduces the turbine stresses is proposed in [14] by means of variable droop control in each one. Another two proposals

[13, 15] have been found that perform a reserve sharing among the turbines in order to take advantage of the highest wind speeds. Nonetheless, it is noticeable that these proposals do not deal with the cost that the power reserve involves to wind power producers, nor with the uncertainty involved when using wind energy.

Differently, this paper addresses the question: What is the cost of curtailing power to the WPP under a risk metric, and which factors do most affect the profit loss? In this regard, the first contribution of this paper to the existing literature is the revision of wind power primary reserve capabilities of a WPP under a risk measure. Wind power production is subject to uncertainty, and therefore the primary reserve cannot be firm. This is in contrast with the conventional thermal generation, where the ISO is fundamentally concerned with the amount of available power reserve. Failure to provide it from a committed generator is considered a contingency, for which appropriate rescheduling is in order. In the case of wind power production, however, the ISO cannot rely on a WPP with high certainty, and it therefore seems reasonable that it not only be informed about the WPP reserve levels but also about its reliability. In order to quantify that reliability, in Section 2.1 the value-at-risk (VaR) will be investigated as a possible risk measure of the available power reserve. The VaR concept is borrowed from the financial context, where it has been widely employed to quantify the risk of financial loss of an investment. Our claim is that—as an upper percentil of a distribution—it can be equally employed to represent the confidence in power availability upon a frequency event, and not only currency losses. (Yet, it will be made evident that the confidence level has opposite meaning in the reserve problem to that of the financial framework.) Though easy to understand and simple to use, we will move to argue in Section 2.2 that the VaR will prove to be a bad choice in the reserve scheduling risk measurement, and that the conditional VaR (CVaR) is an acceptable "upgrade" that ensures a more representative measure of risk over a wider range of reserve levels and reliabilities. We emphasize that the risk measure is applied not to a financial context, on which it exists extensive literature, but to the specific characteristics of power production by wind generators, which is largely biased towards extreme values. This bias produces a distinctive distribution of probability [16], which makes it arguable the use of CVaR, as we defend in Section 2.2. We acknowledge that other recent works have also employed the CVaR in the wind power generation context. However, the use of CVaR has been again employed to measure the *economic* loss risk (as a weighted part of the objective function of an optimization problem), as in financial contexts: see for instance [17, 18, 19]. Differently, we employ CVaR as a constraint to the power reserve, to ensure a given generator output under a given confidence level.

A second contribution of this paper is the analysis of the optimality of the distribution of reserves in a WPP. Other recent works have addressed the problem of wind power reserve optimization from the point of view of dispatching [20, 21] or of reducing the deviation penalties [12], but without addressing the optimal internal scheduling in a WPP that leads to a

economical loss minimization. Specifically, Section 2.3.1 features a lossless approach to find the optimal scheduling, which is later upgraded (Section 2.3.2) to incorporate line losses through a two-level program including a non-derivative load power flow (LPF). These two approaches serve to identify the optimal allocation of curtailed power in a WPP considering wind speed profiles, energy conversion characteristics, and properly the WPP layout. In the end, the solutions of those programs will be analyzed in Section 3 for a range of scenarios to reveal the existence of allocation patterns.

The results of Section 3 will show that in some cases the best (i.e., optimal) allocation of reserves inside a WPP will entail putting one or more particular generator off-line. Consequently, these results must be analyzed with caution, because this seems to not fit into the conventional regulation that the reserve should be spinning and automatic. To be consistent, the ISO should have to accept quick start-up units for primary frequency regulation, which is not the established practice. Nonetheless, we emphasize that the results shown in Section 3 are those that provide the optimal, ideal curtailment of every individual generator belonging to a WPP. But also, this paper discusses the conceptual rules to find the sub-optimals, which do not require putting generators off-line, and therefore would be acceptable under the current operational rules. Also, we must note that this paper is based on the assumption that the wind speed distribution is known, either in parametric or in non-parametric form. This would make the methodology discussed in the next sections useful for planning purposes, when a WPP reserve capability is valued. But it is interesting to see that the same methodology can be applied to assessing the value of a given forecast, when this is made in the form of a probability distribution. In such a case, of interest for the ahead planning of the ISO, the translation of the concepts developed in this paper would be straightforward: under the forecast distribution of wind speed, the program would give the necessary curtailment of each generator inside the WPP to achieve an expected total power reserve at a given level of confidence.

2. METHODOLOGY

2.1. Value-at-risk

The α-VaR is an upper percentil of a loss distribution function, representing the upper estimate of losses that will not be exceeded with a confidence level α. In a financial context, the VaR provides investors with an estimate of the maximum losses they will face through a position in a financial portfolio, depending on the level of confidence they want.

The *loss function* is central to this risk assessment approach. In most financial settings it gives the profit loss associated to a position in a given portfolio; hence its name. Similarly, this paper considers the reserved wind power as an opportunity loss to the WPP operator, which can be therefore represented by a loss function $f : \mathbb{R}^{N\times n_G} \times \mathbb{R}^{n_G} \mapsto \mathbb{R}^N$. To account

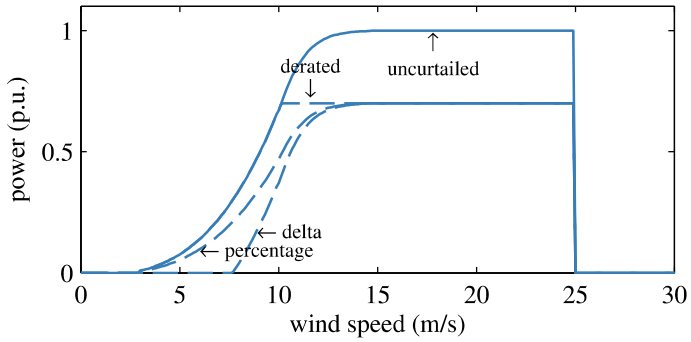

Figure 1. Characteristic conversion curve of the 600-kW Enercon E40 (solid line). De-loaded characteristics for 20% power reserve are also shown (dashed lines).

for the loss originated by the curtailment, this function maps wind speed and allocated curtailment following a de-loading policy into loss power. Specifically:

$$f(\boldsymbol{\xi}, \mathbf{w}) = \sum_{i=1}^{n_{\mathrm{G}}} \left[g(\mathbf{w}_i, 0) - g(\mathbf{w}_i, \xi_i) \right], \tag{1}$$

where $\mathbf{w} = (\mathbf{w}_1, \ldots, \mathbf{w}_{n_{\mathrm{G}}})$, and $\mathbf{w}_i$ is the N-observation vector of wind speed at the i-th site, of the n_{G} WPP turbines. Vector $\boldsymbol{\xi} = (\xi_1, \ldots, \xi_{n_{\mathrm{G}}})$ determines the portion of power that is reserved in each generator—that is, it defines the degree of power curtailment of every generator. Function $g : \mathbb{R}^{N \times n_{\mathrm{G}}} \times \mathbb{R}^{n_{\mathrm{G}}} \mapsto \mathbb{R}^N$ maps wind speed into wind power, considering the curtailment ξ_i. Basically three options are reported in the literature to specify this function: delta, derated, and percentage (Fig. 1). In this paper, only the delta function is considered, mindful that the application of the other two approaches is straightforward. Particularly, the specification of g employed in this paper for each i-th generator is:

$$g(\mathbf{w}_i, \xi_i) = \max\{0, g(\mathbf{w}_i, 0) - \xi_i\}. \tag{2}$$

If $\xi_i = 0$, the power curtailment is null and the power conversion follows the nominal characteristic of the turbine, $g(\mathbf{w}_i, 0)$, as provided by the manufacturer. (In this paper we employed the 600-kW Enercon E40 turbine, with its characteristic nominal curve represented in Fig. 1. The detailed piecewise specification of $g(\mathbf{w}_i, 0)$ can be found in [22].) On the other hand, entries of $\boldsymbol{\xi}$ equal to one mean that the corresponding generators are separated from the grid, meaning that all the available power is reserved.

For a particular reserve policy specified by a given $\boldsymbol{\xi}$, the vectors of wind speed are mapped by the loss function (1) into reserved power. Accordingly, because wind speed is a random variable, the reserved power, R, is also a random variable with a VaR that is defined as

$$VaR_\alpha = \min \left\{ r \geq 0 \,:\, \mathrm{pr}\left\{ R > r \right\} \leq 1 - \alpha \right\}. \tag{3}$$

The previous definition of VaR is employed in financial contexts, but it has two major issues in the power reserve problem approached in this paper. First, the interpretation of the confidence level is different. It is common practice in financial analysis to set high confidence levels: for instance, $\alpha = 95\%$ indicates that the investor will not incur in losses greater than $VaR_{95\%}$, with a 95% probability. However, the power reserve problem has two intervening agents, not one, and this importantly varies the interpretation of the quantile. The power reserve is a loss to the WPP operator (the first intervening agent), because that power cannot be sold. It is requested, however, by the ISO (the second agent). If in parallel to the financial practice the ISO sets a high $\alpha = 95\%$, it implies that the reserved power will not exceed $VaR_{95\%}$ a 95% of times. But statistically speaking this means that *the reserved power might perfectly be zero 95% of times*. However, for reliability purposes the ISO will be surely willing that the reserved power be *in excess* of the requested reserve 95% of times. Therefore, from the ISO viewpoint it is $\beta = 1 - \alpha$ the true confidence level. An $\alpha = 5\%$, meaning $\beta = 95\%$, tells the ISO that the reserve power will be in excess of $VaR_{5\%}$ 95% of times.

2.2. CVaR

The second issue with VaR is related to some undesirable limiting characteristics when analyzing general distributions [23, 24]. In the case of wind power production the limitations are so severe, indeed, that in what follows we argue that VaR as a measure of reserved power problem is impractical; leading in fact to wrong assessments.

To show it, we processed the wind speed records of two adjacent wind sites. The data come from the NREL dataset in [25]. Specifically, we employed the averaged 1-hour records of sites 25228 and 25194 of year 2006, with the frequency distribution contrasted in Fig. 2a.

The mapping of wind speed into wind power is nonlinear and piecewise defined, as shown in Fig. 1. This produces an uneven transformation of wind speed into wind power, with ensuing frequency distributions that typically exhibit two visible "spikes", at 0.0 and 1.0 p.u (Fig. 3b). The spike at 0.0 p.u. reveals the null power production when the wind speed falls below the cut-in (2.5 m/s) or exceeds the cut-off (25 m/s) speeds (see Fig. 1). The spike at 1.0 p.u. is a consequence of winds at speeds between the rated (15 m/s) and the cut-off wind speeds. Visibly, site 25194 with higher mean wind speed produces a larger spike at 1.0 p.u. than site 25228.

If the loss function (1) is computed for every possible curtailment, represented by the pair $(\xi_{25194}, \xi_{25228})$, and the VaR is computed through (3) for each realization of f, the result is similar to that in Fig. 3a. Variants occur when the confidence level is varied (making more or less visible the plateau) or when other wind distributions are employed , but eventually Fig. 3a proves to be a generic representation.

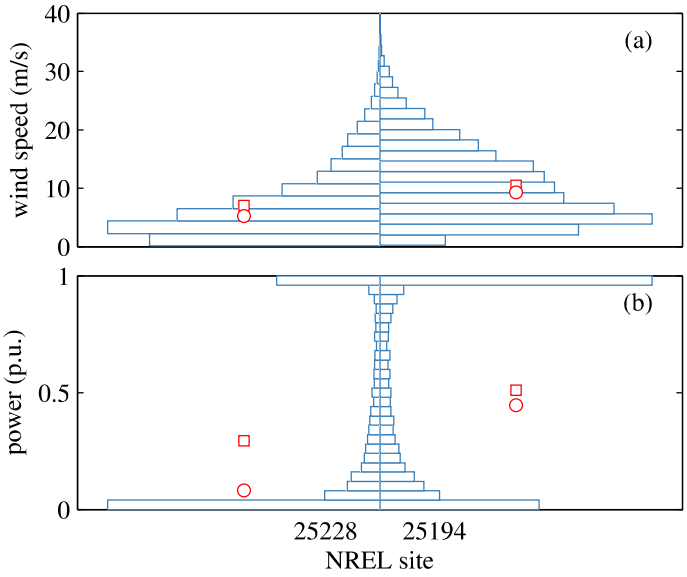

Figure 2. Frequency comparison of random variables based on the evaluation of NREL datasets of sites id. 25228 and 25194. (a) Wind speed. (b) Wind power after processing wind speed through the Enercon E40 conversion function of Fig. 1 (full conversion, without reserved power). The markers are the sample means (□) and medians (○).

For general distributions it is known that VaR is non-convex [23, 24]; what can be readily observed in Fig. 3a with specific regard to the reserve problem approached in this paper. Although this is an added complication in approaching optimization problems, because it implies using global search algorithms, it does not pose an insurmountable difficulty. (Indeed, later in this paper a global optimization procedure is proposed to investigate the occurrence of multiple solutions.) The most relevant limitation, however, is that VaR only considers the risk at an α-percentile of the loss distribution, hence disregarding the magnitude of the losses in the α-tail of the loss distribution. That is, it disregards the worst $1-\alpha$ portion of scenarios; producing the visible plateau when the reserve request is relatively demanding. (An examination of the curves of reserved power as a function of β shows that the plateau is a consequence of the discontinuity appearing at the maximum power reserve, similar to that provoking the spikes at 1.0 p.u. in Fig. 3b.) Therefore, this implies that the VaR measure—which is the value of power reserve of the WPP—does not depend on the degree of curtailment exceeding a given value. Referring to Fig. 3a, for values of ξ_{25194} and ξ_{25228} greater than approximately 0.4, the obtained reserve will be always around 0.5 p.u.; even if both generators are completely unloaded. This interpretation makes the VaR obviously impractical in the power reserve context.

To overcome the shortcomings of VaR, Rockafellar and Uryasev developed the concept of conditional value-at-risk (CVaR), based on the VaR, in [26]; gaining since wide acceptation in the financial framework. The CVaR is the weighted

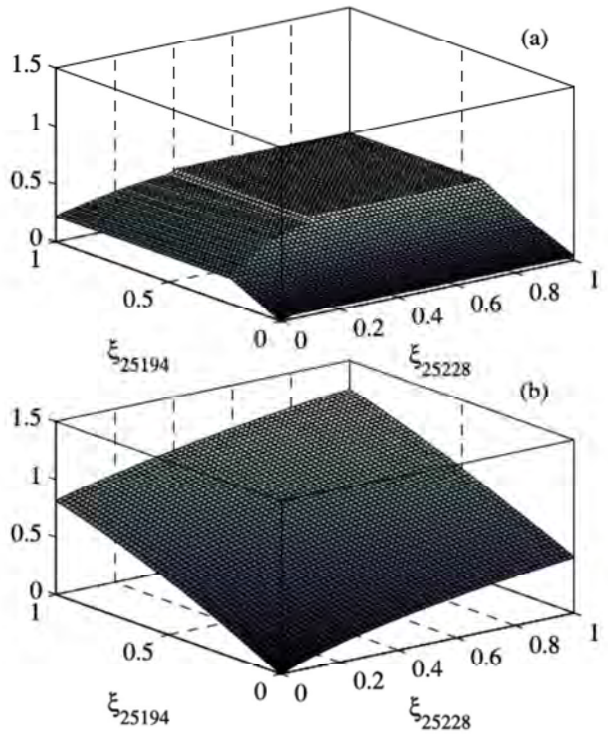

Figure 3. VaR (a) and CVaR (b) in p.u. under different curtailments of Enercon E40 wind power, subject to winds of sites 25228 and 25194 of NREL dataset. ISO confidence level is $\beta = 0.6$.

average of the losses exceeding the VaR and the VaR itself:

$$CVaR_\alpha = \frac{1}{1-\alpha} \int_{f(\boldsymbol{\xi},\mathbf{w}) \geq VaR_\alpha} f(\boldsymbol{\xi}, \mathbf{w}) p(\mathbf{w}) \, \mathrm{d}\mathbf{w}. \tag{4}$$

Because the CVaR averages VaR and exceeding reserves, it accounts not only for the lowest bound of reserves (as VaR does), but also for the extent of reserves beyond the threshold provided by VaR. CVaR and VaR are equivalent when the loss distribution is normal, but not so in other instances—as the one presented in this paper—where CVaR outperforms VaR in tractability and coherence [27]. And more importantly, CVaR can be readily incorporated into minimization problems in a simple manner, as discussed in [26], where the authors demonstrated that (4) can be inferred in discrete form as

$$CVaR_\alpha = \underset{\boldsymbol{\xi}, VaR}{\operatorname{argmin}} \left[VaR_\alpha + \frac{1}{(1-\alpha)N} \sum_{k=1}^{N} \max\{f(\boldsymbol{\xi}, \mathbf{w}) - VaR_\alpha, 0\} \right]. \tag{5}$$

Ultimately, the representation of CVaR is markedly different from that of VaR, as observed in Fig. 3. As commented above, the reserve specification leading to Fig. 3 was selected as an instance where non-convexity and the VaR plateau were evident. For low values of β and reserve, the VaR representation would be equivalent to that of CVaR (both panels

of Fig. 3 would be identical). However, in the case presented in Fig. 3 both representations coincide only in a tiny portion at the origin—where the curtailments of both generators are almost negligible. Beyond that domain, CVaR improves the assessment of the reserves by eliminating the plateau and the non-convex area.

2.3. Optimal distribution of the reserve

2.3.1. Lossless approach

Once made a reserve request, it is the role of the WPP operator to self-schedule the power production. Because the WPP consists of distributed generators of possibly different power outputs, the question faced by the operator is how to distribute the reserve in the least costly way, provided that the required power and confidence levels are met.

The scheduling question can be easily cast into an optimization problem:

$$\begin{aligned} \max_{\boldsymbol{\xi}} \quad & \mathcal{E}_t \left[\pi_t \sum_{i=1}^{n_\mathrm{G}} g(\mathbf{w}_i, \xi_i) \right] \\ \text{s.t.} \quad & CVaR_\alpha \geq r_\mathrm{ISO} \\ & \xi_i \in [0,1],\ i = 1, \ldots, n_\mathrm{G}, \end{aligned} \tag{6}$$

where $CVaR_\alpha$ is defined as in (5), employing the loss function (1); r_ISO is the reserve level agreed upon with the ISO at a confidence level $\alpha = 1 - \beta$; π_t is the feed-in price at observation t; and $\mathcal{E}_t$ is the statistical average over the sample.

The program (6) employs the wind speed samples at every i-th site as inputs. These n_G samples are mapped into reserved wind power through (2). The mapping depends on the decision vector $\boldsymbol{\xi} = (\xi_1, \ldots, \xi_{n_\mathrm{G}})$. Over the iterative process, tentative sets of curtailments $\boldsymbol{\xi}$ are tested, producing different reserve profiles. The loss function (1) gathers the $N \times n_\mathrm{G}$ reserved power samples into one sample of size N. This sample is employed to compute the CVaR and check whether the inequality constraint holds—that is, whether the CVaR as risk-valued measure of power reserve exceeds the ISO request. Ultimately, the optimal solution $\boldsymbol{\xi}^*$ will maximize the WPP income by energy sales.

2.3.2. BFS-based approach

The program (6) incorporates the two conflicting interests: maximization of returns by energy sales (for the WPP operator) and a reliable provision of a minimum reserve (for the ISO). It may be argued, however, that the solution to the previous problem might not be the best. The obtained $\boldsymbol{\xi}^*$ might well unload the generators nearest to the WPP grid connection. This raises the concern that the generators providing the more line losses would be the most productive.

An alternative approach to (6) includes a more involved calculation of the objective function. Rather than computing the economic profit as the sum of produced power at each generator (times the price of electricity), it does so through the

solution of a power flow. This change in approach consequently entails important changes in the program work flow, as discussed next.

Because the WPP is a radial system, algorithms of the backward-forward sweep (BFS) type seem appropriate. These are derivative free algorithms that besides simple have proven to improve tractability in the power flow calculation of radial systems, with fast convergence [28]. However, the solution method makes it necessary approaching the optimization problem as a two-level program. The top level accounts for the curtailment calculation, with $\boldsymbol{\xi}$ as decision variable; while the bottom level, the BFS algorithm, provides the power flow solution for the prospective $\boldsymbol{\xi}$'s. This two-level approach is because BFS algorithm consists in making successive sweeps of the WPP network to eventually find a stable solution of the node voltages. Over the backward sweep, the branch currents are computed from the node injected currents through the use of KCL at each node, starting at the most remote ones. The injected currents are calculated assuming that the node voltages are known and using the power injected by the generators, which are curtailed as dictated by the top-level program. Over the forward sweep the voltages are updated starting from grid-connected node and assuming that the branch currents—calculated over the backward sweep—are correct now.

We employed the algorithm described in the flowchart represented in Fig. 4. The key matrix in this approach is the node-edge incidence matrix, $\boldsymbol{\Gamma}$, of a directed graph that represents the distribution network. In a general case, it is a matrix of size $n_{\mathrm{N}} \times n_{\mathrm{B}}$ (number of nodes $\times$ number of branches). In the particular case analyzed in this paper, however, $\boldsymbol{\Gamma}$ is a square matrix of size $(n_{\mathrm{N}}-1)\times(n_{\mathrm{N}}-1)$, because (i) a purely radial system has one less branch than the number of nodes, and (ii) the grid-interface node is left out of the sweeps. (This particularity of being square shows later to be crucial to specify the compact formulation.) If $\boldsymbol{\Gamma} = [\gamma_{ij}]$, the matrix has the following structure [29, p.37]:

- $\gamma_{ij} = 1$ if branch j is incident at node i and is directed away from it.
- $\gamma_{ij} = -1$ if branch j is incident at node i and is directed towards it.
- $\gamma_{ij} = 0$ if branch j is not incident at node i.

With this formulation about the grid structure, let $\mathbf{I} = (\mathbf{I}_2, \ldots, \mathbf{I}_{n_{\mathrm{N}}})$ be the vector of complex currents drawn from the $n_{\mathrm{N}} - 1$ nodes (again the grid-interface is discarded). In [29, Sect. 2.2], Chen showed that $\mathbf{I}$ relates to the branch current vector $\mathbf{I}^{\mathrm{b}} = (\mathbf{I}^{\mathrm{b}}_1, \ldots, \mathbf{I}^{\mathrm{b}}_{n_{\mathrm{N}}-1})$ through the incidence matrix: $\mathbf{I} = \boldsymbol{\Gamma}^t\mathbf{I}^{\mathrm{b}}$, where subscript t means transpose. Moreover, Chen showed that the same incidence matrix relates the voltage drops in the branches to voltage drops in the nodes: $\Delta\mathbf{U}' = \boldsymbol{\Gamma}^{-1}\mathbf{U}^{\mathrm{b}}$, where $\Delta\mathbf{U} = (\Delta\mathbf{U}_2, \ldots, \Delta\mathbf{U}_{n_{\mathrm{N}}})$ gathers the complex voltage drops in the nodes, and $\mathbf{U}^{\mathrm{b}} = (\mathbf{U}^{\mathrm{b}}_1, \ldots, \mathbf{U}^{\mathrm{b}}_{n_{\mathrm{N}}-1})$ are the voltage drops in the branches. If now $\mathbf{Z}$ is introduced as the vector of line impedances, so that its elements are sorted in the same order as the branch voltages and currents in $\mathbf{U}^{\mathrm{b}}$ and $\mathbf{I}^{\mathrm{b}}$, it follows that $\mathbf{U}^{\mathrm{b}} =$

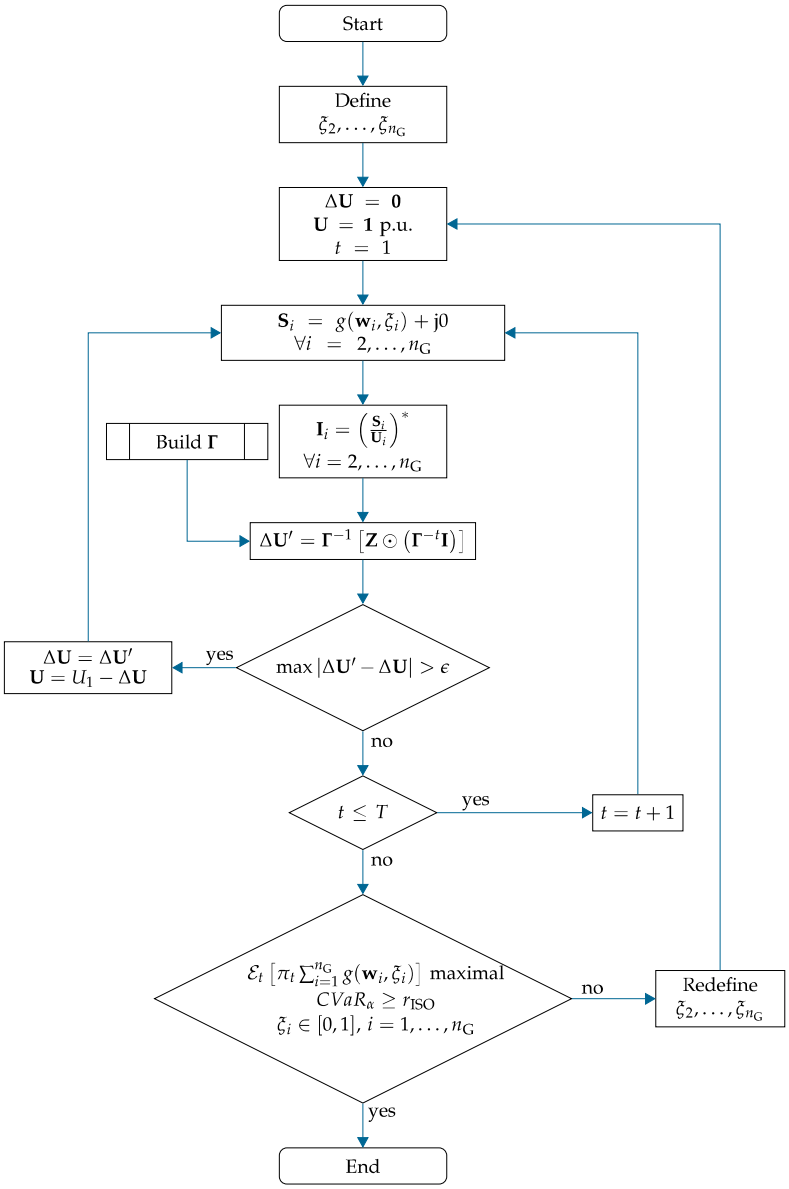

Figure 4. BFS-based optimization approach.

$\mathbf{Z} \odot \mathbf{I}^{\mathrm{b}}$; where the operator $\odot$ stands for the element-wise multiplication of two vectors: $(a_1, \ldots, a_n) \odot (b_1, \ldots, b_n) = (a_1 b_1, \ldots, a_n b_n)$.

The considerations above eventually allow, by rearranging and combining the previous components, producing the said compact formula for the voltage deviations:

$$\Delta\mathbf{U}' = \mathbf{\Gamma}^{-1}\left[\mathbf{Z} \odot \left(\mathbf{\Gamma}^{-t}\mathbf{I}\right)\right], \tag{7}$$

where the superscript $-t$ indicates inverse transpose.

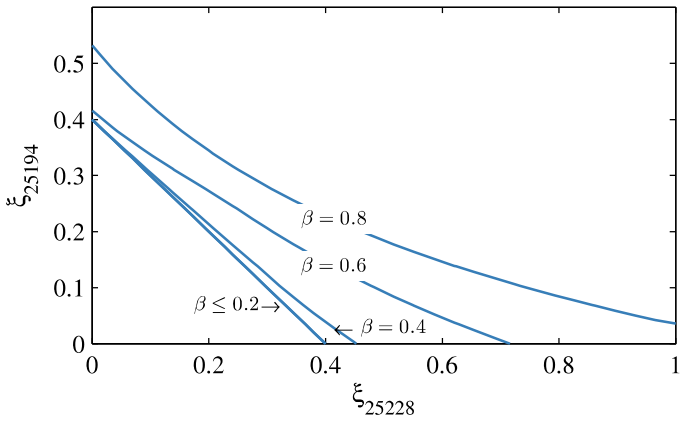

Figure 5. Isolines of ISO confidence level for $CVaR = 0.4$ p.u.

Clearly this second formulation is computationally more intensive than the original (6). Ultimately the difference resides only in the specification of the objective and loss functions; but not in the problem structure. In (6) they are expressed in closed form as the sums of incomes and power curtailment, respectively. Quite differently, in the second approach the BFS algorithm is questioned about the available and reserved powers at the grid-connected node upon each iteration. And though an implementation employing matrix algebra (we employed a variation of [30]) shows a marked improvement in speed, still the need for several sweeps at each candidate $\boldsymbol{\xi}$ considerably slows down this version of optimal program.

3. RESULTS AND DISCUSSION

3.1. Significance of β on the actual curtailment.

The introduction of a risk measure to specify the reserve reliability definitely complicates the reserve allocation among generators. This is exemplified in Fig. 5. Low levels of confidence (in Fig. 5, $\beta \leq 0.2$) cause that the curtailments follow the simple rule $\xi_{25194} + \xi_{25228} = r_{\mathrm{ISO}}$. There is no preference in such cases regarding the distribution of the total curtailment—either generator 25194 or the 25228 can be indistinctly curtailed in 0.4 p.u.; or for instance the requested reserve can be equally divided between both, 0.2 p.u. each. This easy rule changes, however, when in search of more reliability β is increased. It then follows that $\xi_{25194} + \xi_{25228} > r_{\mathrm{ISO}}$, implying that the loss of power production is more than what nominally declares r_{ISO}.

In fact, the excess of $\xi_{25194} + \xi_{25228}$ over r_{ISO} depends on the reserve allocation policy. Generator 25228 has the lowest capacity factor (CF) and consequently requires a relatively larger curtailment than generator 25194 to achieve the reserve goal. This is so because the CF is indeed a measure of the statistical production of a given generator. When the

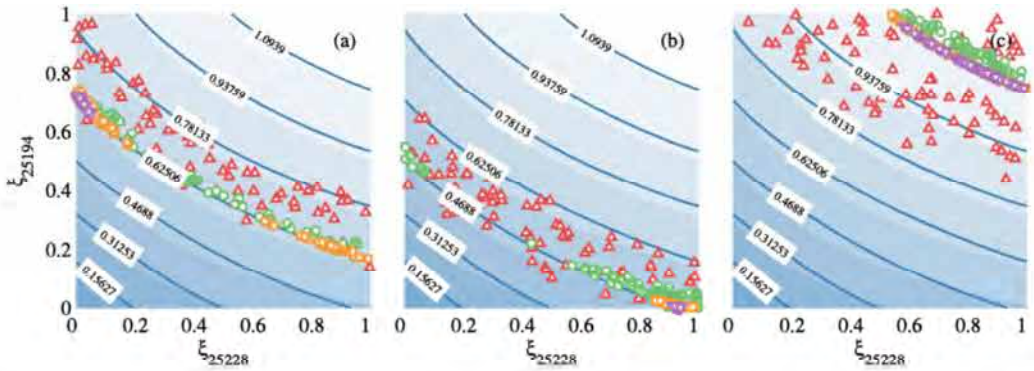

Figure 6. Convergence of the DEA. Generations shown are 2nd (△), 4th (○), 7th (□), and 12th (▽). Confidence level is $\beta = 0.6$. Levels of reserved power, CVaR, are indicated with labels. Also levels of profit from wind power sales are represented by the shaded areas (the darkest shade corresponds to the highest profit). The requested reserve is (a) 0.625 p.u., (b) 0.469 p.u., and (c) 1.094 p.u.

CF is relatively high, it means that the generator spends relatively more hours a year in the production interval (with wind speeds between cut-in and furling values). This in turn may be interpreted as a larger confidence in that generator if the power reserve were requested. It ensues that the CF gives an easy indication about which are the generators more suitable to provide an amount of reserve with higher confidence. But also it is noticeable that the curtailment is not linear in the sense that it cannot be optimally distributed in inverse proportion to the CF. The curtailment is sensitive to the weight given to each generator in building the reserve. Thus, if greater emphasis is put in the generator with lowest CF, the amount of curtailment increases more than proportionally. This sensitivity is increased when β is also increased—as an amplification of the lower confidence in generator 25228. (Clearly the sensitivity of the curtailment of one generator to changes in the other is readily investigated through the slope of the isoline. Only for $\beta \leq 0.2$, where the isoline slope is constantly -1 are the curtailment increments equal. For larger β the slope is progressively reduced, indicating a larger sensitivity of ξ_{25228} to changes in ξ_{25194}.) In this respect it is noticeable that the generator 25194, with the largest CF, can give the full requested reserve 0.4 p.u. individually, though incurring in an slight over-reserve: $\xi_{25194} = 0.529$ ($\beta = 0.8$). Not so the generator 25228 of lower CF, which is not capable of giving the reserve individually—it requires the support of the other generator, with $\xi_{25194} = 0.036$ when $\xi_{25228} = 1.000$. The amount of curtailment over r_{ISO} in this case is noticeable, $\xi_{25194} + \xi_{25228} = 1.036 \approx 2.6 \times r_{\mathrm{ISO}}$.

3.2. Uniqueness of the optimal solution

First indications are that the CVaR-based problem is convex and can be solved by for instance interior-point algorithms (IPA). However, our preliminary tests showed inconsistent values of $\boldsymbol{\xi}^*$: slight changes in the reserve request at high β

would often produce drastically different $\boldsymbol{\xi}^*$. To further investigate this issue—namely the possibility of local maxima—we resorted to a global optimization algorithm. Particularly, the differential evolution algorithm (DEA) published in [31] seemed appropriate: importantly it allows not only the specification of bounds of ξ_i, but also of complex constraints; and reportedly it features improved accuracy. The use of this DEA would eventually prove to be valuable for validating and illustrating the existence a Pareto front, justifying the inconsistence in the solutions offered by the IPA.

The panels of Fig. 6 provide insight on the optimal solution manifold through simple demonstrations of the performance of the constrained DEA. Again we employed a two-dimensional approach based on the data presented in Fig. 3. The first case (Fig. 6a) explores the convergence of the DEA in an "intermediate" reserve request: the combination of r_{ISO} and β is demanding, but not excessively. In this case, it is noticeable how the DEA progresses to the maximum of the objective function by successively pruning the individuals with the lowest profit (those furthest to the northeast of the $CVaR_{0.4} = 0.625$ p.u. line) and those infeasible individuals that violate the CVaR constraint (below the line). Eventually, the optimal solution is found at the upper extreme of the CVaR line. This means that generator 25228 is left uncurtailed. By contrast, when the r_{ISO} is less demanding (Fig. 6b) the algorithm populations evolve towards the opposite extreme: the optimal solution implies that the most profitable generator 25194 remains now uncurtailed.

The situation is quite different when the reserve requirements are high (Fig. 6c). In such cases, the constraint and objective isolines practically coincide. The constrained DEA requires comparatively a much larger number of iterations to reach the solution. (In Fig. 6c after 12 generations, the individuals are still widely spread over the constraint. The algorithm has already stripped the population from the least profitable individuals and from those violating the constraint; but it has a difficult time discerning an optimal solution.) It is in these cases when the interior-point algorithms get stuck at points close to the initial guesses. However, this analysis demonstrates that in any case those different solutions are all equivalent, and hence Pareto-optimal; implying that an optimization program is indeed nonessential to distribute high reserve requests, because ultimately the problem consists in finding *any* combination of $\boldsymbol{\xi}$ that meets the CVaR constraint.

3.3. Extension to WPP

In what follows the analysis focuses on high-dimensional problems, also considering the spatial location of the generators. For that purpose we defined a WPP using the 33-node system detailed in [32]. Except for the tie-node 1, we assumed that each node had a wind generator, with wind speed profiles obtained from the NREL data base [25], with codes 24483 through 24499, 24430 through 24433, 24680 through 24682, and 24563 through 24570 (see also [33]). What comes next

Table I. Capacity factors and Weibull scale (m/s) and shape of the wind speed profiles represented in Fig. 7a.

Node	1	2	3	4	5	6	7	8
CF	44.0%	43.8%	44.4%	44.1%	44.2%	43.8%	42.9%	42.3%
Scale	9.24	9.20	9.34	9.32	9.40	9.39	9.31	9.31
Shape	1.55	1.54	1.53	1.52	1.50	1.47	1.46	1.43
Node	9	10	11	12	13	14	15	16
CF	41.7%	40.2%	39.4%	37.6%	37.6%	36.6%	36.3%	36.2%
Scale	9.34	9.12	9.19	8.80	8.90	8.61	8.51	8.45
Shape	1.40	1.37	1.33	1.30	1.30	1.30	1.33	1.35
Node	17	18	19	20	21	22	23	24
CF	35.7%	40.9%	40.7%	40.4%	40.4%	49.6%	47.8%	49.8%
Scale	8.30	8.80	8.82	8.82	8.88	10.28	9.97	10.40
Shape	1.37	1.47	1.47	1.45	1.43	1.88	1.88	1.85
Node	25	26	27	28	29	30	31	32
CF	45.8%	44.5%	43.7%	42.4%	40.0%	38.5%	36.9%	36.6%
Scale	9.83	9.63	9.62	9.62	9.24	9.26	8.88	8.95
Shape	1.48	1.45	1.41	1.35	1.30	1.24	1.25	1.25

about the particularities of establishing optimal distributions of reserve requests is for a 24-hour wind profile described in Fig. 7a and Table I.

3.3.1. Equivalences and discrepancies between algorithms

The tabulated results in Fig. 8 assess the convergence characteristics of the different optimization procedures discussed previously. Listed top-down below each node are the values of curtailments obtained for scenarios 1 through 5 of Table II. For clarity when a generator output is left uncurtailed, we have drawn a dash rather than writing 0.00. This seems to improve the visibility of generators affected by curtailment. Exceptionally, the figures below node 1 (the grid-connection node, devoid of wind generation) represent the sum of curtailments of each scenario, $\sum_{i=2}^{33} \xi_i$.

The first three rows show the curtailment obtained for a high confidence level ($\beta = 0.8$). The first row is the best solution produced by the constrained DEA after 5×10^5 fitness evaluations (as suggested in [31]); and second and third rows show

Table II. List of scenarios.

Scenario	β	r_{ISO} (p.u.)	π_t	Algorithm	Return (€/MWh)
1	0.8	6.4	FiT	DE + BFS	-14.1
2	0.8	6.4	FiT	IP+ BFS	-14.1
3	0.8	6.4	FiT	IP+ BFS	-14.1
4	0.6	12.8	FiT	IP+ BFS	-10.0
5	0.6	12.8	FiT	DE	-12.4
6	0.2	6.4	FiT	DE + BFS	-16.6
7	0.4	6.4	FiT	DE + BFS	-16.2
8	0.6	6.4	FiT	DE + BFS	-15.2
9	0.8	6.4	FiT	DE + BFS	-14.1
10	0.6	12.8	FiT	DE + BFS	-10.1
11	0.8	12.8	FiT	DE + BFS	-8.5
12	0.8	3.2	FiT	DE + BFS	-16.4
13	0.8	3.2	Spot, 1/24	DE + BFS	-667.7
14	0.8	3.2	Spot, 1/25	DE + BFS	-329.5

the solution to the same problem employing an IPA with different initial guesses. Though the contour conditions are the same, the three scenarios yield different schedulings. For instance, full curtailment is exchanged between generators 18 and 28, depending on the IPA run. Also the sums of curtailments, $\sum_{i=2}^{33} \xi_i$ under node 1, are slightly different. However, essentially the three tests yield the same value of the objective function (14.1 €/MWh, Table II). On the whole the three schedulings are equivalent; thus corroborating the hypothesis of existence of a Pareto front also in high-dimensional problems under high reserve requirements.

In previous section it was raised the concern about possible differences in reserve allocations between the simple program (6) and an expanded two-level, BFS-based program. This issue is investigated through scenarios 4 and 5 of Table II, with the results in the last two rows of Fig. 8. (Now with a reduced $\beta = 0.6$ the solutions are unique, leading to a fair comparison of reserve allocations between the two investigated programs.) The solutions are visibly different. To account for the line losses and their impact on the reserve uncertainty, the BFS-based program returns a larger curtailment: as shown by $\sum_{i=2}^{33} \xi_i$ under node 1, it is 2.6 p.u. in excess of that produced by the simpler program (6). This entails that

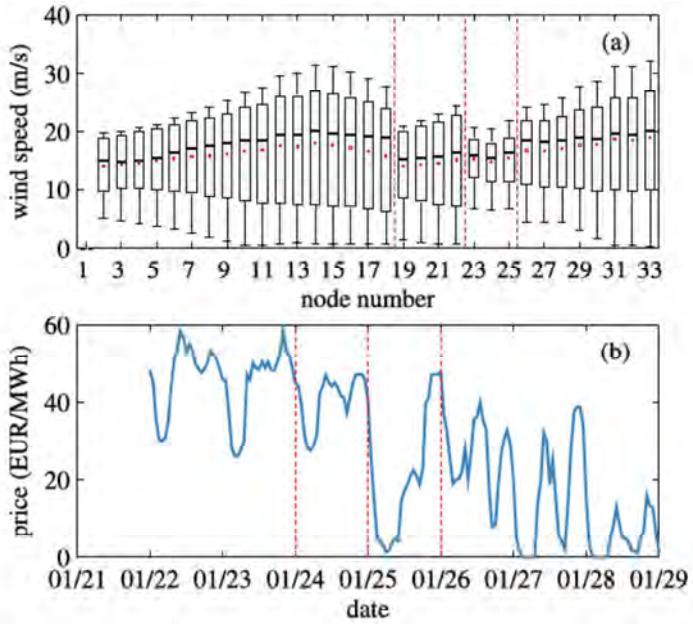

Figure 7. (a) Tukey's box plots of wind speed distributions of the 33-node WPP. Vertical lines demarcate the four sections or branches of the network (see Fig. 8). (b) Samples of Spanish electricity spot price for the FiP analysis.

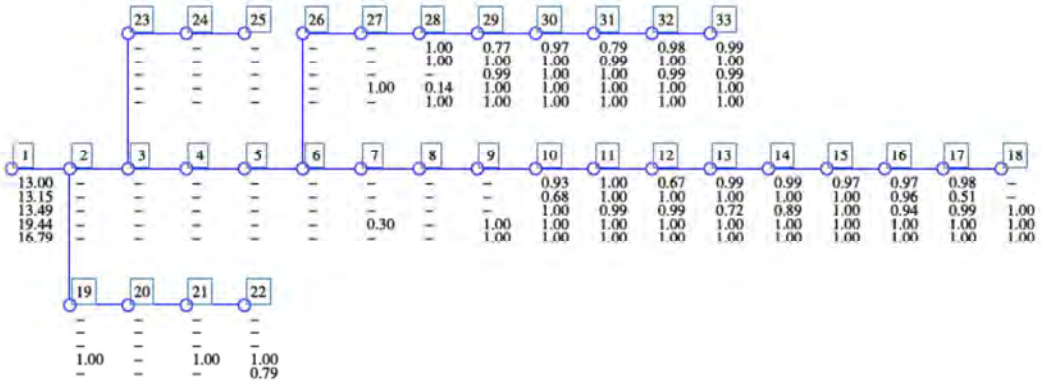

Figure 8. Curtailment results under different algorithm comparisons, corresponding to scenarios 1 through 5 of Table II.

the BFS-based program recruits two more generators in the lowest branch, in nodes 19 and 21, as well as in nodes 7 and 27. Because the reserve request in these two scenarios was so high ($r_{\mathrm{ISO}} = 12.8 = 0.4 \times 32$ p.u.; hence requesting a 40% reserve to each generator), the DEA had already committed a large part of the production to reserves, and the commitment of additional generation produces a relevant loss of income. It must be stressed out, however, that this is an extreme case designed to reveal an important discrepancy between both approaches. When contrarily r_{ISO} is more moderate, our results show that the discrepancy is not so relevant, and that therefore the less computationally intensive approach (6) can be

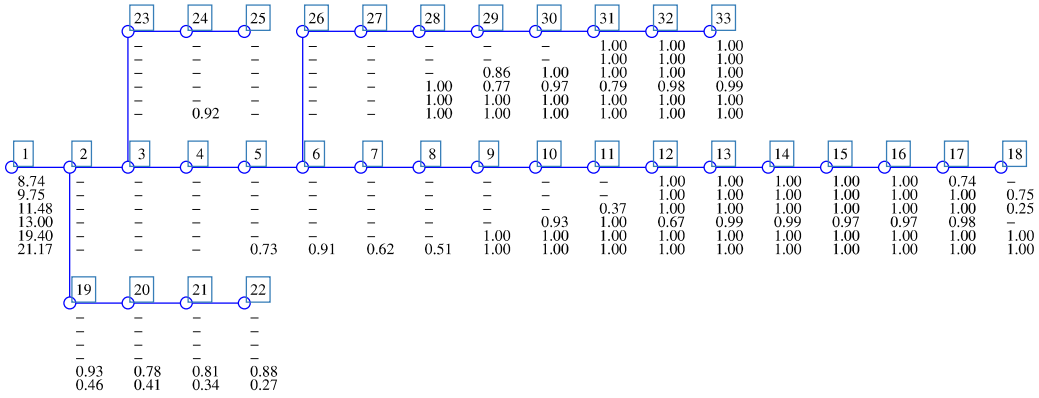

Figure 9. Impact of reserve requirements, corresponding to scenarios 6 through 11 of Table II.

Table III. Even distribution of the reserve request in Table II.

Scenario	6	7	8	9	10	11
CVaR (p.u.)	6.40	6.37	6.06	5.57	11.62	10.77
Return (€/MWh)	-14.1	-14.1	-14.1	-14.1	-10.1	-10.1

Table IV. Even distribution of the required curtailments to ensure proper confidence in Table II (see node 1 of Fig. 9).

Scenario	6	7	8	9	10	11
CVaR (p.u.)	8.74	9.62	10.51	10.92	17.11	16.02
Return (€/MWh)	-13.48	-12.84	-11.79	-10.87	-7.10	-6.06

equivalently used. In a Intel(R) Core(TM) i7-3770 CPU machine, of 3.40 GHz, with 8 GB RAM installed, the average times for solving scenarios 4 and 5 are relevantly different: 1.7 and 29.7 seconds, respectively.

3.3.2. Significance of β and r_{ISO}

Further insight on the impact of reserve requirements—power and confidence levels—on the optimal reserve allocation is provided in Fig. 9. Results are ordered top-down from less to more demanding requirements (scenarios 6 through 11, Table II). As expected, the figures indicate that increasing β again implies a larger estimate of the reserve. For the less demanding reserve (first row, $\beta = 0.2$ and $r_{\mathrm{ISO}} = 6.4$ p.u.) the allocation follows the pattern discussed above: generators are preferably put off-line, completely curtailed, to meet the power allotment. For the scenario with largest reserve reliability (forth row, $\beta = 0.8$) the solution is Pareto optimal and partial curtailments are allowed.

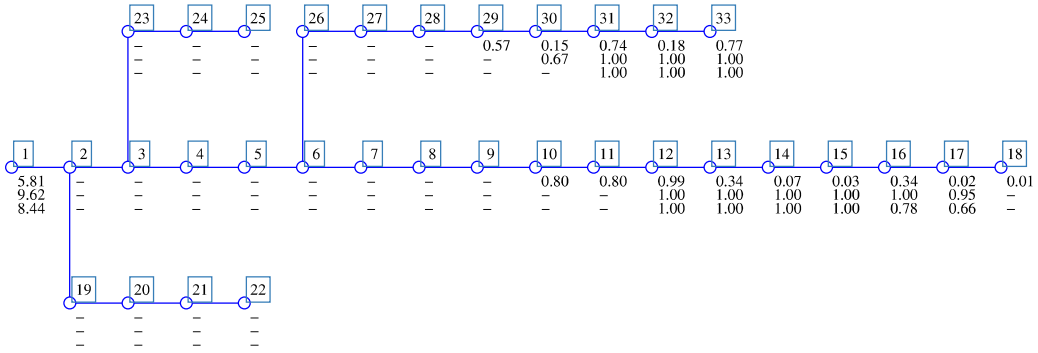

Figure 10. Price influence, corresponding to scenarios 12 through 14 of Table II. Scenario 13 and 14 employ the prices of January 24 and 25, 2015, respectively (Fig. 7b).

The impact of an optimal distribution of the curtailment can be additionally investigated using the data in Tables III and IV. Table III lists the value of the economical return when each of the 32 generators is curtailed by 0.2 p.u. (scenarios 6 through 9, where the request is $32 \times 0.2 = 6.4$ p.u.) and by 0.4 p.u. (scenarios 10 and 11, where the request is $32 \times 0.4 = 12.8$ p.u.). Because scenarios 6 through 11 are all evenly curtailed by a total 6.4 p.u., the only variable changing is the confidence level. Clearly, when β rises from 0.2 to 0.8 the return is the same (same curtailment) but the CVaR falls down below the requested 6.4 p.u., except in the least demanding scenario 6. The same reasoning can be applied to scenarios 11 and 12.

Contrary to the data in Table III, where the reserve request is kept constant, and the validity of the solution is degraded by the increasing level of confidence, in Table IV we ensured that the confidence β and CVaR were the required, by using the results of curtailment plotted under node 1 in Fig. 9. We again divided the values evenly. Now, for instance, scenario 8 requiring a total curtailment of 13.49 p.u. to ensure $r_{\mathrm{ISO}} = 6.4p.u.$ under $\beta = 0.6$ was tested by curtailing each of the 32 generators $13.49/32 = 0.42$ p.u. This yielded a CVaR equal to 10.51, which is higher than r_{ISO}, but also than that obtained by optimally allocating the reserves. As a consequence, the return drops from 15.20 to 11.79 €/MWh.

As for the "geographical" allocation of the reserves, also a pattern is revealed. Starting around the generators with largest CF (nodes 14 and 33), the reserves are allocated by recruiting highly productive generators; which, as commented above, are put off-line when β is reduced. The progression of curtailments follows this pattern, and only for the most demanding scenario 11 is a generator o branch 23–25 recruited (a possibility included in the Pareto optimal set for such a high demand).

3.3.3. Price policies

The previous analyses were made on the basis of a feed-in tariff (FiT) payment—a policy mechanism through which the WPP receives a fixed price per produced MWh, stipulated at the start of the contract. (For simplicity we assumed 1 €/MWh.) In theses cases the time of day is irrelevant concerning the expected revenues. Contrarily, under a feed-in premium (FiP) mechanism the WPP receives a payment composed of the spot price plus a stipulated premium on top (which we will assume for simplicity to be zero). To conclude this section, the need to consider the price structure in the objective function is corroborated through the results shown in Fig. 10. As shown in Fig. 10, the variability in prices makes the curtailments again more extreme than in the FiT scheme to increase profitability. Also the clear difference between both days prices makes it necessary to readjust the scheduling to improve profitability.

4. CONCLUSIONS

This paper has focused on the interpretation of power reserves in a WPP by elaborating an optimization approach, with a valuation of the reserve capability under a risk metric.

We have shown that the confidence level, β, has a fundamental relevance in the scheduling of reserves. When it is low—meaning that the ISO cannot rely on the WPP for a firm reserve—it happens that (i) the total curtailment matches the minimum ISO request, but (ii) only one specific curtailment pattern produces the financial optimality of the WPP. This unique point consists in putting off-line generators rather than scheduling partial curtailments. Contrarily, when high reliability in the reserve is offered to the ISO, it happens that (i) an over-reserve in the WPP is indicated, actually implying an extra loss of profit to the WPP; and (ii) a Pareto optimality exists in the distribution of reserves for maximum profitability, with solutions allowing partial curtailments of generators.

The previous conclusions also hold for high reserve requests. Particularly we can argue that either increasing the curtailment or the confidence levels yields similar results; and thus the level of confidence can be treated as an extra request of reserve, with direct economic interpretation.

Regarding the optimization programs proposed in this paper, we can conclude that fast interior-point algorithms are adequate, remaining mindful that a Pareto front exists under high reserve requirements. As for the use of LPF algorithms our results showed that, under the prevalence of the capacity factor as the driving criterion for distributing the reserve in the WPP, the inclusion of line losses is not necessary except for high reserve demands.

5. ACKNOWLEDGMENT

This work has been carried out inside the Unit UFI11/16 (UPV/EHU) and supported by the Basque University System IT394-10 and by the Government of the Basque Country (ETORTEK) as FUTUREGRIDS-2020 (IE14-389).

REFERENCES

1. Ela E, Milligan M, Kirby B. Operating Reserves and Variable Generation: A comprehensive review of current strategies, studies, and fundamental research on the impact that increased penetration of variable renewable generation has on power system operating reserves. *Technical Report* 2011.
2. Yan R, Saha TK. A new tool to estimate maximum wind power penetration level: In perspective of frequency response adequacy. *Applied Energy* sep 2015; **154**:209–220, doi:10.1016/j.apenergy.2015.04.085. URL http://www.sciencedirect.com/science/article/pii/S0306261915005486.
3. Díaz-González F, Hau M, Sumper A, Gomis-Bellmunt O. Participation of wind power plants in system frequency control: Review of grid code requirements and control methods. *Renewable and Sustainable Energy Reviews* jun 2014; **34**:551–564, doi:10.1016/j.rser.2014.03.040. URL http://www.sciencedirect.com/science/article/pii/S1364032114002019.
4. Tsili M, Papathanassiou S. A review of grid code technical requirements for wind farms 2009, doi:10.1049/iet-rpg.2008.0070.
5. Koliou E, Eid C, Chaves-Ávila JP, Hakvoort RA. Demand response in liberalized electricity markets: Analysis of aggregated load participation in the German balancing mechanism. *Energy* jul 2014; **71**:245–254, doi:10.1016/j.energy.2014.04.067. URL http://www.sciencedirect.com/science/article/pii/S0360544214004800.
6. Driesen J, De Vos K. Active participation of wind power in operating reserves. *IET Renewable Power Generation* aug 2015; **9**(6):566–575, doi:10.1049/iet-rpg.2014.0142. URL http://digital-library.theiet.org/content/journals/10.1049/iet-rpg.2014.0142.
7. Rodrigues E, Osório G, Godina R, Bizuayehu A, Lujano-Rojas J, Catalão J. Grid code reinforcements for deeper renewable generation in insular energy systems. *Renewable and Sustainable Energy Reviews* jan 2016; **53**:163–177, doi:10.1016/j.rser.2015.08.047. URL http://www.sciencedirect.com/science/article/pii/S1364032115009107.

8. Cardell JB, Anderson CL. A Flexible Dispatch Margin for Wind Integration. *IEEE Transactions on Power Systems* may 2015; **30**(3):1501–1510, doi:10.1109/TPWRS.2014.2337662. URL http://ieeexplore.ieee.org/articleDetails.jsp?arnumber=6877721.

9. Jeong Y, Johnson K, Fleming P. Comparison and testing of power reserve control strategies for grid-connected wind turbines. *Wind Energy* mar 2014; **17**(3):343–358, doi:10.1002/we.1578. URL http://doi.wiley.com/10.1002/we.1578.

10. Fleming PA, Aho J, Buckspan A, Ela E, Zhang Y, Gevorgian V, Scholbrock A, Pao L, Damiani R. Effects of power reserve control on wind turbine structural loading. *Wind Energy* mar 2015; :n/a–n/adoi:10.1002/we.1844. URL http://doi.wiley.com/10.1002/we.1844.

11. Yingcheng X, Nengling T. Review of contribution to frequency control through variable speed wind turbine 2011, doi:10.1016/j.renene.2010.11.009.

12. Soares T, Pinson P, Jensen TV, Morais H. Optimal Offering Strategies for Wind Power in Energy and Primary Reserve Markets. *IEEE Transactions on Sustainable Energy* 2016; **PP**(99):1–10, doi:10.1109/TSTE.2016.2516767. URL http://ieeexplore.ieee.org/lpdocs/epic03/wrapper.htm?arnumber=7399764.

13. Attya AB, Hartkopf T. Wind farms dispatching to manage the activation of frequency support algorithms embedded in connected wind turbines. *International Journal of Electrical Power and Energy Systems* 2013; **53**:923–936, doi:10.1016/j.ijepes.2013.06.011.

14. Vidyanandan KV, Senroy N. Primary frequency regulation by deloaded wind turbines using variable droop. *IEEE Transactions on Power Systems* may 2013; **28**(2):837–846, doi:10.1109/TPWRS.2012.2208233. URL http://ieeexplore.ieee.org/lpdocs/epic03/wrapper.htm?arnumber=6265353.

15. Wang Y, Bayem H, Giralt-Devant M, Silva V, Guillaud X, Francois B. Methods for Assessing Available Wind Primary Power Reserve. *IEEE Transactions on Sustainable Energy* jan 2015; **6**(1):272–280, doi:10.1109/TSTE.2014.2369235. URL http://ieeexplore.ieee.org/lpdocs/epic03/wrapper.htm?arnumber=6983475.

16. Díaz G, Gómez-Aleixandre J, Coto J. Statistical characterization of aggregated wind power from small clusters of generators. *International Journal of Electrical Power & Energy Systems* nov 2014; **62**:273–283, doi:10.1016/j.ijepes.2014.04.033. URL http://www.sciencedirect.com/science/article/pii/S0142061514002282.

17. Baringo L, Conejo AJ. Offering Strategy of Wind-Power Producer: A Multi-Stage Risk-Constrained Approach. *IEEE Transactions on Power Systems* mar 2016; **31**(2):1420–1429, doi:10.1109/TPWRS.2015.2411332. URL http://ieeexplore.ieee.org/lpdocs/epic03/wrapper.htm?arnumber=7089322.

18. Dai T, Qiao W. Optimal Bidding Strategy of a Strategic Wind Power Producer in the Short-Term Market. *IEEE Transactions on Sustainable Energy* jul 2015; **6**(3):707–719, doi:10.1109/TSTE.2015.2406322. URL http://ieeexplore.ieee.org/lpdocs/epic03/wrapper.htm?arnumber=7078933.

19. Rabiee A, Soroudi A, Keane A. Risk-Averse Preventive Voltage Control of AC/DC Power Systems Including Wind Power Generation. *IEEE Transactions on Sustainable Energy* oct 2015; **6**(4):1494–1505, doi:10.1109/TSTE.2015.2451511. URL http://ieeexplore.ieee.org/lpdocs/epic03/wrapper.htm?arnumber=7166342.

20. Hedayati-Mehdiabadi M, Zhang J, Hedman KW. Wind Power Dispatch Margin for Flexible Energy and Reserve Scheduling With Increased Wind Generation. *IEEE Transactions on Sustainable Energy* oct 2015; **6**(4):1543–1552, doi:10.1109/TSTE.2015.2455552. URL http://ieeexplore.ieee.org/lpdocs/epic03/wrapper.htm?arnumber=7202870.

21. Ebrahimi F, Khayatiyan A, Farjah E. A novel optimizing power control strategy for centralized wind farm control system. *Renewable Energy* feb 2016; **86**:399–408, doi:10.1016/j.renene.2015.07.101. URL http://www.sciencedirect.com/science/article/pii/S0960148115301968.

22. Diaz G, Abd-el Motaleb AM, Mier V. On the Capacity Factor of Distributed Wind Generation in Droop-Regulated Microgrids. *IEEE Transactions on Power Systems* 2012; **28**(2):1–1, doi:10.1109/TPWRS.2012.2222941. URL http://ieeexplore.ieee.org/lpdocs/epic03/wrapper.htm?arnumber=6353619.

23. Larsen N, Mausser H, Uryasev S. Algorithms for optimization of value-at-risk. *Financial Engineering, E-commerce and Supply Chain*. 2002. URL http://www.pacca.info/public/files/docs/public/finance/ActiveRiskManagement/Uryasev-AlgorithmsOptimizationVaR.pdf.

24. Forghieri S. Portfolio optimization using CVaR jul 2014. URL http://tesi.eprints.luiss.it/12528/1/forghieri-simone-tesi-2014.pdf.

25. National Renewable Energy Laboratory. NREL wind dataset. URL http://wind.nrel.gov/Web{_}nrel/.

26. Rockafellar R, Uryasev S. Optimization of conditional value-at-risk. *Journal of risk* 2000; URL http://www.pacca.info/public/files/docs/public/finance/ActiveRiskManagement/UryasevRockafellar-OptimizationCVaR.pdf.

27. Rockafellar R, Uryasev S. Conditional value-at-risk for general loss distributions. *Journal of Banking & Finance* jul 2002; **26**(7):1443–1471, doi:10.1016/S0378-4266(02)00271-6. URL http://www.sciencedirect.com/science/article/pii/S0378426602002716.

28. Eminoglu U, Hocaoglu MH. Distribution Systems Forward/Backward Sweep-based Power Flow Algorithms: A Review and Comparison Study. *Electric Power Components and Systems* dec 2008; **37**(1):91–110, doi:10.1080/15325000802322046. URL http://dx.doi.org/10.1080/15325000802322046.

29. Chen WK. *Applied Graph Theory: Graphs and Electrical Networks*, vol. 28. Elsevier, 2014. URL https://books.google.com/books?id=wYqjBQAAQBAJ{&}pgis=1.

30. Jen-Hao Teng. A direct approach for distribution system load flow solutions. *IEEE Transactions on Power Delivery* jul 2003; **18**(3):882–887, doi:10.1109/TPWRD.2003.813818. URL http://ieeexplore.ieee.org/lpdocs/epic03/wrapper.htm?arnumber=1208371.

31. Jia G, Wang Y, Cai Z, Jin Y. An improved (μ+λ)-constrained differential evolution for constrained optimization. *Information Sciences* feb 2013; **222**:302–322, doi:10.1016/j.ins.2012.01.017. URL http://www.sciencedirect.com/science/article/pii/S0020025512000369.

32. Baran M, Wu F. Network reconfiguration in distribution systems for loss reduction and load balancing. *IEEE Transactions on Power Delivery* apr 1989; **4**(2):1401–1407, doi:10.1109/61.25627. URL http://ieeexplore.ieee.org/lpdocs/epic03/wrapper.htm?arnumber=25627.

33. Díaz G, Gómez-Aleixandre J, Coto J. Wind power scenario generation through state-space specifications for uncertainty analysis of wind power plants. *Applied Energy* jan 2016; **162**:21–30, doi:10.1016/j.apenergy.2015.10.052. URL http://www.sciencedirect.com/science/article/pii/S0306261915012799.